Ion energy distribution function in dual-frequency rf capacitively coupled discharges: Analytical model

M. Olevanov, O. Proshina, T. Rakhimova, and D. Voloshin
Skobeltsyn Institute of Nuclear Physics, Lomonosov Moscow State University, Leninskie Gory, Moscow 119991, Russia
(Received 3 April 2008; published 12 August 2008)

An analytical approach is used to calculate an ion energy distribution function (IEDF) in a dual frequency (DF) collisionless rf discharge in argon. Three possible limit regimes for frequency relations in the DF discharge are discussed. The analytical IEDF is obtained for the intermediate-frequency case, which is most applicable in plasma-processing technologies. The analytical expressions for an ion spectrum width as well as for the minimum and maximum ion energies are derived. The analytical theory is compared with a particle-in-cell Monte Carlo numerical simulation and also with the results of a semianalytical model.

DOI: 10.1103/PhysRevE.78.026404 PACS number(s): 52.80.Pi, 52.65.Rr, 52.65.Pp

I. INTRODUCTION

Low pressure capacitively coupled radio frequency plasmas (CCP) have been used successfully for several decades in the microelectronics industry for plasma etching, deposition, and surface treatment. Recently, a new generation of CCP plasma driven by two rf sources, dual-frequency capacitive coupled plasma (DF CCP), was developed to realize more flexible control of the ion fluxes and ion energies at the substrates [1–5]. The experimental and theoretical study of DF CCP plasma is of great interest due to its wide application for anisotropic and selective etching [6–21]. The use of two widely different rf frequencies allows the separate control of a plasma density and the energies of ions impinging on a substrate. The plasma density is determined by the input power at high frequency (HF), and the ion energy by the input power at low frequency (LF). In that way, it is possible to achieve more flexible control of the plasma parameters and etching characteristics. However, the DF plasma is a nonlinear system and coupling between frequencies can influence the perfect and precise control of the ion flux and the ion spectrum on the sample. At present, both theoretical [6–20] and experimental [2–5,21] investigations are being performed in order to find the optimum discharge parameters for frequency decoupling.

The ion energy and angular distribution function (IEDF, IADF) at the substrate play a crucial role in plasma processing because of the strong influence of the surface reactions. A kinetic approach based on the particle-in-cell with the Monte Carlo collision (PIC MCC) method [22,23] is mainly used for the numerical simulation of DF CCP discharges and IEDF calculations. In [7–12,20,24–27] numerous simulations of symmetric [7,9,10] and asymmetric [8] dual-frequency [7–14,26,27] and single-frequency [7,24] discharges were performed in pure argon [11–14,24] as well as in complex gas mixtures such as Ar/CF_4 and $Ar/CF_4/N_2$ [7–10,26,27]. The self-consisted PIC MCC model is the most correct one but takes a lot of computational time. Therefore, one needs some methods for the quick analysis of the plasma and IEDF properties in the given physical conditions. Also, pure numerical simulations lose some lucidity in the details and interrelation of physical processes.

In a number of works, semianalytical models of electrode sheath are applied for the IEDF calculations. In these models, an ion spectrum is obtained by the integration of the equation of ion motion in the specified electric field $E(x,t)$ [20,28–30] using the Monte Carlo method or from the numerical solution of the system of equations taking into account the electric field distribution [16,31–33]. In recent papers, self-consisted hybrid models of the dual-frequency sheath [34] or the whole discharge [35] have been introduced, coupled with the Monte Carlo method for the investigation of the IEDF and ion angle distribution.

Though the methods mentioned above reduce the computational time and shed light on the discharge organization, the development of pure analytical approaches is also necessary. Analytical models of the discharge sheaths, IEDF formation, and the whole discharge allow fast analysis of the plasma properties and are required for their forecasting with changing of the external parameters. However, the development of the analytical models has turned out to be a complicated task for the strongly nonlinear systems under consideration. In this case, the essential simplifications should be applied, and the correctness of such simplifications requires additional validation in any specific case.

Ions gain their energy mainly in the electrode sheath region, where the electric field is much higher than in the plasma bulk region. So, the spatialtemporal characteristics of the sheath will determine the IEDF structure.

The temporal characteristic of the sheath is a relation of the ion transit time through the sheath τ_{ion} and the rf period τ_{rf}. There are two limit regimes for the single frequency (SF) discharges: the low-frequency (LF) regime ($\tau_{\mathrm{ion}} \ll \tau_{\mathrm{rf}}$) and the high-frequency (HF) regime ($\tau_{\mathrm{ion}} \gg \tau_{\mathrm{rf}}$). In the HF regime, ions cross the sheath for many periods of the electric field and they respond to the average sheath potential drop. In the collisionless sheath, the IEDF in the HF regime should be close to a monoenergetic function. In the LF regime, ions cross the sheath for a small part of the rf period and trace the instantaneous value of the sheath electric field. So, the final ion energy at the electrode will depend strongly on the phase of the sheath electric field at which the ions come into the sheath.

In DF discharges with the low ω_l and high ω_h frequencies, there are three limit regimes: the high frequency (HF) $\tau_{\mathrm{ion}} \gg \tau_l \gg \tau_h$, the intermediate frequency (IF) $\tau_h \ll \tau_{\mathrm{ion}} \ll \tau_l$, and the low frequency (LF) $\tau_{\mathrm{ion}} \ll \tau_h \ll \tau_l$. The frequency regime will be discussed in more detail in Sec. II.

The essential contribution to the development of the analytical sheath models of the SF discharge was made in [36–38]. In [17,18], the model [37] was extended for the DF case. The main assumption of these models is the ion motion in the average electric field (HF limit). A global analytical model of the DF discharge is presented in [19]. This model is based on an assumption of the constant profile of the ion concentration.

In [39], an analytical sheath model for DF CCP plasma is introduced for the case in which an ion is postulated to respond to an instantaneous electric field. This model gives an expression for the sheath potential and the ion density in the sheath, but a study of the IEDF in the frame of this model has not yet been performed.

The analytical IEDF in the single-frequency (SF) discharge within a high-frequency limit is presented in [40–43]. This is the case when the ion transit time is much higher than the rf period, and the energy of the ions impinging a substrate is determined by the average plasma potential. Nevertheless, taking into account the high-frequency modulations leads to the weak bimodal form of the ion spectrum. In [7], the approach described in [40–43] was extended to the DF case, and the analytical IEDF in the DF discharge was obtained for the case when the ion transit time through the sheath is higher than the low-frequency (LF) period.

In [44], a method for computing the IEDF based on the concept of the effective voltage seen by ions crossing the sheath is introduced. The effective voltage is found from the analytical expression for the sheath voltage from model [17] through the transfer function for the Fourier transform of this sheath voltage. The parameters for the transfer function were found by fitting the analytical results to the PIC MCC simulation. A detailed review of different approaches and numerical models for IEDF is presented in [45].

Though dual-frequency discharges are often operated under conditions close to the IF limit (2 MHz–27 MHz, 1.76 MHz–81 MHz) the analytical expression for the IEDF form in the DF discharges was not received in this case. For the derivation of the analytic form of the IEDF, which can qualitatively give the features of the ion spectra in the IF limit, the simplified sheath model was used in this paper. In the frame of this model, the analytic expressions for the IEDF, peak position, and IEDF width were obtained for the first time. The comparison of the analytical and numerical IEDFs shows that, in spite of the simplifications made, the analytical approach gives the main properties of the ion spectra in the IF limit.

In the present work, the analytical expressions for the IEDF in SF and DF cases are obtained in the framework of the linear sheath model [19]. In the SF discharge, the low-frequency limit was considered when the ion transit time is much lower than the rf period. In the DF discharge, the intermediate-frequency case was considered when the ion transit time through the sheath is much lower than the LF period and much higher than the HF period. This regime is of great interest since it is often realized in real processing conditions. The different limit regimes for frequency relations are discussed in detail in Sec. II, as well as the main principles of the present analytical model. The analytical expressions for the IEDF in the SF and DF cases are derived in Sec. III. The results of the analytical model were validated using the self-consistent and semianalytical numerical simulations of the DF discharge. The details of the numerical models used are described in Sec. IV. The analytical calculations are compared with the numerical results in Sec. V. The main conclusions are summarized in Sec. VI. All the simulations are performed for the DF discharge in pure Ar at a rf frequency ratio of 1.76 MHz/81 MHz.

II. MAIN PRINCIPLES OF THE ANALYTICAL MODEL AND CLASSIFICATION OF THE FREQUENCY REGIMES

Before the IEDF description in the SF and DF discharges, we will first describe briefly the basic assumptions and principles of the analytical sheath model. The expression used for the electric field distribution in the sheath follows the linear sheath model as follows:

$$E(x,t) = \begin{cases} \dfrac{2V_0}{s_m^2}[x - s_1(t)], & x < s_1 \\ 0, & x > s_1, \end{cases} \tag{1}$$

where s_m is the maximum sheath width, and V_0 is the applied electrode voltage. In the DF case, $V_0 = V_l + V_h$, where V_l and V_h are the voltages at low and high frequency, respectively. $s_1(t)$ is the moving bulk-sheath boundary, which is evaluated by the formula

$$s_1(t) = \frac{s_m}{2}(1 + \cos \omega t) \tag{2}$$

in the SF case, and

$$s_1(t) = \frac{s_m}{2}\left(1 + \frac{V_l}{V_l + V_h}\cos(\omega_l t) + \frac{V_h}{V_l + V_h}\cos(\omega_h t)\right) \tag{3}$$

in the DF case. Equation (3) can be derived from the global model of the DF discharge (see, for example, [19,20]). The linear approximation of the electric field in Eq. (1) conforms to the assumption of the homogeneous ion density profile in the sheath [36].

The ion energy spectrum is determined by many discharge parameters, such as the sheath structure, the presence of ion-neutral collisions in the sheath, the dependence of ion-neutral collision cross sections on the ion energy, the ion velocity distribution at the plasma-sheath boundary, and the multicomponent ion composition in the case of complex gas mixtures. Therefore, the analytical calculation of the IEDF is difficult to perform in a general case. Nevertheless, the analytical IEDF can be derived in a number of limiting cases that are physically important for the better understanding of the IEDF formation mechanism. One of these cases is a collisionless mode at low gas pressures, when the ions free path λ is much larger than the maximum sheath width s_m ($s_m \ll \lambda$). The collision case takes place at $s_m \gg \lambda$.

Let us estimate the lower limit of Ar pressures at which ion collisions with neutrals have an influence on the ion energy spectrum. The results of [20] for the DF discharge are used for further estimations and calculations. From the PIC

MCC calculations [20], the sheath width $s_m \sim 0.2$ cm in a pressure range of 20–45 mTorr and at a gap of 2.4 cm. The charge transfer cross section is $\sigma_{ct} \cong 4-8\times10^{-15}$ cm^2 for argon [46], thus collisions begin to play a role at concentrations of Ar $n_0 \geqslant 0.6-1.2\times10^{15}$ cm^{-3}, i.e., at pressures of $p \geqslant 20-40$ mTorr. Thereby, the sheath is weakly collisional in the conditions of study.

As noted above, another key parameter that determines the ions energy spectrum is the relation between the ion transit time through the sheath τ_i and the rf period τ_{rf}. In addition τ_i strongly depends on the electric field in the sheath and the corresponding ion density. There are two limit regimes for the SF discharges—the low-frequency (LF) regime

$$\tau_i \ll \tau_{rf}, \quad \omega \ll \omega_i, \quad \omega\tau_i \ll 1, \tag{4}$$

and the high-frequency (HF) regime

$$\tau_i \gg \tau_{rf}, \quad \omega \gg \omega_i, \quad \omega\tau_i \gg 1, \tag{5}$$

where the plasma frequency is

$$\omega_i^2 = \frac{4\pi e^2 n_s}{M}, \tag{6}$$

and n_s is the typical ion concentration in the sheath. In the HF regime, ions take many rf cycles to cross the sheath and the ion energy at the electrode corresponds to the average plasma potential U_p. In the present sheath model, the average plasma potential is evaluated by the formula [47]

$$U_p = \frac{3}{8} eV_0. \tag{7}$$

In this case, the ion energy spectrum should be close to the monoenergetic one [36,40–43,45,47].

For typical ion concentrations in the sheath of $n_s \sim 10^7-10^9$ cm^{-3} (as resulted from the PIC MCC simulations), we have $\omega_i \sim 10^6-10^7$ s^{-1}. Therefore, at rf frequencies higher than 10 MHz, the HF regime takes place, and the frequency decreasing below 10 MHz results in the gradual transition to the LF regime.

In the DF discharge with the low ω_l and high ω_h frequencies $\omega_l \ll \omega_h$, there are three limit regimes as follows:

$$\text{high frequency (HF)}, \quad \omega_i \ll \omega_l \ll \omega_h, \quad 1 \ll \omega_l\tau_i \ll \omega_h\tau_i, \tag{8}$$

$$\text{intermediate frequency (IF)}, \quad \omega_l \ll \omega_i \ll \omega_h, \quad \omega_l\tau_i \ll 1 \ll \omega_h\tau_i, \tag{9}$$

and

$$\text{low frequency (LF)}, \quad \omega_l \ll \omega_h \ll \omega_i, \quad \omega_l\tau_i \ll \omega_h\tau_i \ll 1. \tag{10}$$

In the first case, the ions' motion occurs in the time-average electric field. As a result, in the collisionless sheath, the ion spectrum should be close to the monoenergetic one with the energy corresponding to the average plasma potential. The analytical IEDF for this case is derived in [7,9]. In the papers referred to above, the less strict inequality was considered $\omega_i < \omega_l \ll \omega_h$ when the IEDF has a weak bimodal shape (at $\omega_i \ll \omega_l \ll \omega_h$, two peaks merge into one). The base approach in [7,9] was the description of the ion motion in the time-average field, and the LF modulation was then taken into account as an amendment.

In contrast to [7,9], we will consider the IF regime $\omega_l \ll \omega_i \ll \omega_h$. This case is most interesting for technological applications since one of the necessary conditions for frequency decoupling is the use of two widely different frequencies.

III. ION ENERGY DISTRIBUTION FUNCTION

A. Single-frequency discharge: Low-frequency regime

Before the derivation of the IEDF in the DF discharge, let us consider the case when inequality (4) is satisfied, i.e., the SF LF regime. This case will be a starting point for the analytical description of the ion spectra in the DF discharge.

The energy gained by the ion in the electric field (1) is

$$\varepsilon_i = e\int_{s_1(\varphi)}^{0} E(x,\varphi)dx = eV_0\frac{s_1^2(\varphi)}{s_m^2}. \tag{11}$$

Here we denoted a field phase $\omega t = \varphi$, in which the ion runs into the movable plasma-sheath boundary $s_1(t)$. The case $\varphi = \pm\pi$ corresponds to $s_1 = 0$; $\varphi = 0$ corresponds to $s_1 = s_m$. Since the LF case is considered, it is assumed that the electric field does not essentially change during the ion transit time through the sheath. As can be seen from expression (11), the variation of the gained energy is controlled only by φ. Then, in order to determine the ion energy distribution function $F(\varepsilon_i)$, one has to find the relative part of the ions entering the plasma boundary s_1 just in this phase.

$$F(\varepsilon_i) = \frac{dN}{d\varepsilon_i} = \frac{dN}{d\varphi}\frac{d\varphi}{d\varepsilon_i}. \tag{12}$$

Here N is the number of ions which entered the sheath. Although the ions come to the maximal sheath boundary s_m at different points in time, they can nevertheless run into the movable boundary at the same field phase φ. This is explained by the initial ion velocity distribution at the plasma-sheath boundary.

Let us designate the IEDF at s_m as $f(\mathbf{v},t)$ and assume it is isotropic and independent of time: $f(\mathbf{v},t) = f(v)$. The total number of ions that enter through the sheath boundary s_m during one cycle of s_1 oscillations is derived by the following expression:

$$N = \Gamma_i\frac{2\pi}{\omega} = \frac{2\pi}{\omega}\int_{\mathbf{v}} v\cos\theta f(v)v^2 dv\sin\theta d\theta\int_{-\pi}^{\pi} d\varphi_0. \tag{13}$$

Here the integration over ion velocities is carried out in spherical coordinates, and the z axis is directed to the left electrode. Γ_i is the ion flux density at the electrode, and φ_0 is the phase in which ions come to the maximal sheath boundary s_m. In addition, φ_0 is directly related to phase φ as follows:

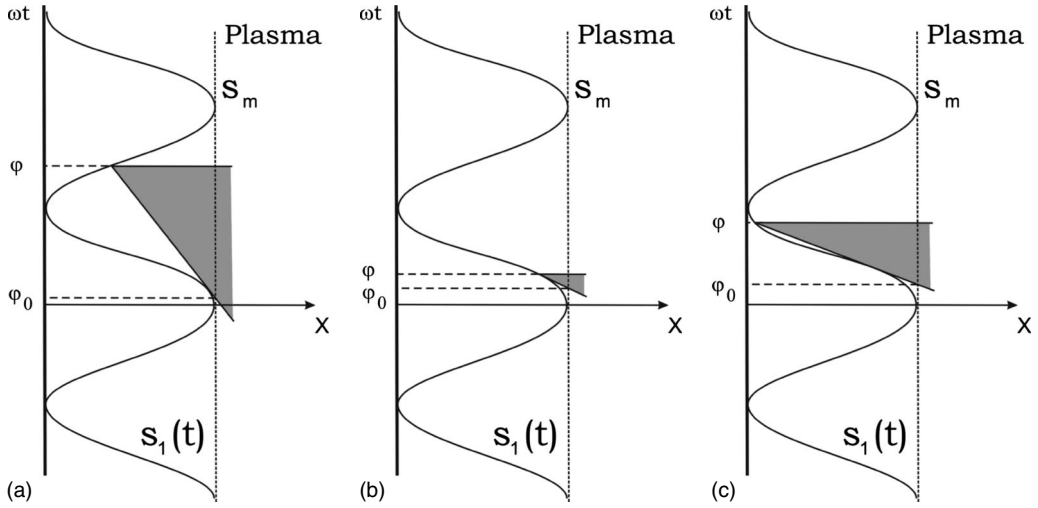

FIG. 1. (a) Diagram of a moving sheath boundary $s_1(t)$ in the SF discharge. Case 1: ions that run into the approaching boundary in phase φ come from the shaded triangle; $\varphi \in -\pi, \ldots, 0$. (b) Diagram of a moving sheath boundary $s_1(t)$ in the SF discharge. Case 2: ions that run into the recessive boundary in phase φ come from the shaded triangle; $s_1(\varphi) \in (s_m/2; s_m)$. (c) Diagram of a moving sheath boundary $s_1(t)$ in the SF discharge. Case 3: ions that run into the recessive boundary in phase φ come from the shaded triangle; $s_1(\varphi) \in (0; s_m/2)$.

$$\varphi_0(v,\theta,\varphi) = \varphi - \frac{\omega[s_m - s_1(\varphi)]}{v\cos\theta}. \tag{14}$$

Then the phase distributions of the ions that run into the movable boundary $s_1(t)$ may be obtained from the following expression:

$$F(\varphi) = \frac{dN}{d\varphi} = C\frac{2\pi}{\omega}\int_{\mathbf{v}} v\cos\theta f(v)v^2 dv \sin\theta d\theta \times \int_{\varphi_0^{\min}}^{\varphi_0^{\max}} \delta(\varsigma - \varphi_0(v,\theta,\varphi))d\varsigma. \tag{15}$$

Here $\varphi_0^{\min}$ and $\varphi_0^{\max}$ are the limited values of φ_0, depending on the ion velocity direction and its absolute value, and C is the normalization factor, defined by the formula

$$\int_{-\pi}^{\pi} F(\varphi)d\varphi = \Gamma_i \frac{2\pi}{\omega}. \tag{16}$$

The internal integral of the delta function in Eq. (15) is equal to

$$\int_{\varphi_0^{\min}}^{\varphi_0^{\max}} \delta(\varsigma - \varphi_0(v,\theta,\varphi))d\varsigma = \begin{cases} 1, & \varphi_0^{\min} < \varphi_0(v,\theta,\varphi) < \varphi_0^{\max} \\ 0, & \varphi_0(v,\theta,\varphi) < \varphi_0^{\min}, \quad \varphi_0(v,\theta,\varphi) > \varphi_0^{\max}. \end{cases} \tag{17}$$

Expression (17) specifies the integration ranges over θ and v. At that, three cases are possible, as can be seen in Figs. 1(a)–1(c).

In the first case [Fig. 1(a)], ions run into the approaching boundary. Here $\varphi \in -\pi, \ldots, 0$, $\varphi_0^{\min} \cong -2\pi$, and $\varphi_0^{\max}$ corresponds to the ion that enters the sheath perpendicularly to the electrode. In this case, the integration ranges are evaluated by the formulas

$$v \geqslant v_{\min} = \frac{\omega[s_m - s_1(\varphi)]}{\varphi + 2\pi}, \tag{18}$$

$$\cos\theta \geqslant \frac{v_{\min}}{v}. \tag{19}$$

$F(\varphi)$ has the following form:

$$F(\varphi) = C\frac{\pi}{\omega}\int_{v_{\min}}^{\infty} v^3 f(v)\left(1 - \frac{v_{\min}^2}{v^2}\right)dv. \tag{20}$$

In the last two cases [Figs. 1(b) and 1(c)], ions run into the recessive boundary. Here $\varphi \in 0, \ldots, \pi$, and $\varphi_0^{\min}$ is determined by a tangent to $s_1(\varphi)$ lined from the point with phase φ. Figure 1(b) illustrates the case when $s_1(\varphi) \in s_m/2, \ldots, s_m$, and the point of tangency coincides with the point φ itself. In this case, formula (18) is replaced by the analogical one as follows:

$$v \geqslant v_{\min} = \frac{\omega s_m}{2}\sin\varphi. \tag{21}$$

In the interval $s_1(\varphi) \in 0, \ldots, s_m/2$, parameter φ_0 varies within the weak bounds [see Fig. 1(c)]; therefore, for further estimations, we will use the value of $\varphi_0^{\min} \cong \pi/2 - 1$ in the boundary phase. Then, instead of Eq. (18), we have the inequality

$$v \geqslant v_{\min} = \frac{\omega[s_m - s_1(\varphi)]}{\varphi - \frac{\pi}{2} + 1}. \tag{22}$$

Expressions (19) and (20) are valid in all three cases. In the studied range of plasma parameters the length of the plasma bulk is higher than the ion free path λ. Namely, in the PIC MCC simulation we consider the DF CCP discharge with an electrode gap of 2.4 cm and a pressure of 20 mTorr. The sheath width s_m is about 0.2 cm. And λ is about 0.15 cm for

the pressure of 20 mTorr. So the sheath is weakly collisional, and the plasma bulk is collisional. These parameter relations allow us to assume the isotropic shape of the IEDF for ions entering the sheath from the plasma bulk. If the Maxwellian distribution of the ion velocities at the sheath boundary s_m is assumed, the expression for $F(\varphi)$ takes the form

$$F(\varphi) = \frac{dN}{d\varphi} = C\frac{\Gamma_i}{\omega}\exp\left(-\frac{m\upsilon_{\min}^2}{2kT_i}\right), \tag{23}$$

where T_i is the characteristic ion temperature in the bulk plasma.

In that way, we have found the portion of ions that run into s_1 just in phase φ. In order to find the IEDF at the electrode, it is necessary to calculate $d\varphi/d\varepsilon_i$, as can be seen from Eq. (12). Let us introduce parameter ξ as follows:

$$\frac{s_1(\varphi)}{s_m} = \xi, \quad 0 \leqslant \xi \leqslant 1. \tag{24}$$

Phase φ is a single-value function of this parameter.

$$\varphi = \pm \arccos(2\xi - 1). \tag{25}$$

We can derive the following expression for ξ from Eq. (11):

$$\xi = \frac{s_1(\varphi)}{s_m} = \sqrt{\frac{\varepsilon_i}{eV_0}}, \quad 0 \leqslant \xi \leqslant 1. \tag{26}$$

Then

$$\frac{d\varphi}{d\varepsilon_i} = \frac{d\varphi}{d\xi}\frac{d\xi}{d\varepsilon_i} = \frac{1}{\sqrt{\xi(1-\xi)}}\frac{1}{2\xi eV_0}. \tag{27}$$

For all three cases described above,

$$\upsilon_{\min} = \omega s_m f_k(\xi), \tag{28}$$

$$\Phi_k(\xi) = \frac{dN}{d\varphi}\frac{d\varphi}{d\varepsilon_i} = C_1(\xi)\exp(-Af_k^2(\xi)), \quad k = 1,2,3, \tag{29}$$

$$f_1(\xi) = \frac{(1-\xi)}{2\pi - \arccos(2\xi - 1)}, \quad f_2(\xi) = \sqrt{\xi(1-\xi)},$$

$$f_3(\xi) = \frac{(1-\xi)}{-\frac{\pi}{2} + 1 + \arccos(2\xi - 1)}, \tag{30}$$

$$C_1(\xi) = \frac{C}{eV_0}\frac{\Gamma_i}{\omega}\frac{1}{2\xi\sqrt{\xi(1-\xi)}}, \quad A = \frac{m\omega^2 s_m^2}{2kT_i} = \frac{\omega^2}{\omega_i^2}\frac{eV_0}{kT_i}. \tag{31}$$

Since, in the interval of $\varphi \in -\pi, \ldots, \pi$, there are two phase points that correspond to the same ion energy, then the IEDF finally takes the form

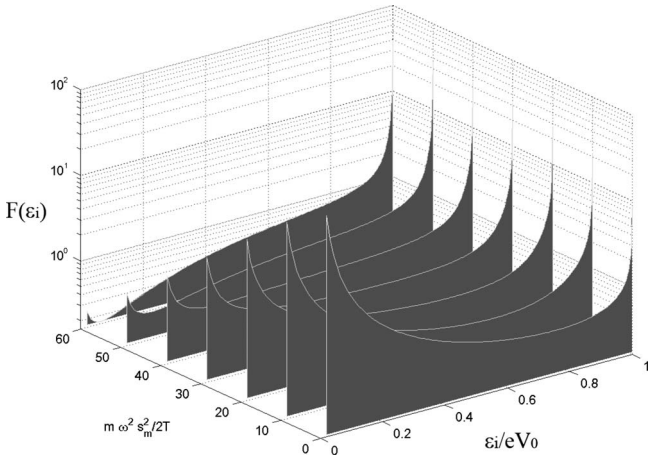

FIG. 2. Analytical IEDF in the SF discharge as a function of normalized ion energy ε_i/eV_0 and parameter $A = m\omega^2 s_m^2/2kT_i = (\omega^2/\omega_i^2)(eV_0/kT_i)$; the low-frequency regime $\omega \ll \omega_i$ is considered.

$$F(\varepsilon_i) = \begin{cases} \Phi_1(\xi) + \Phi_3(\xi), & 0 \leqslant \xi \leqslant \dfrac{1}{2} \\ \Phi_1(\xi) + \Phi_2(\xi), & \dfrac{1}{2} < \xi \leqslant 1. \end{cases} \tag{32}$$

In Eq. (32), term $\Phi_1(\xi)$ represents the ions that run into the approaching sheath boundary, and terms $\Phi_2(\xi)$ and $\Phi_3(\xi)$ correspond to the ions which run into the recessive boundary.

Let us analyze the obtained analytical solution for the IEDF. First, it follows from Eq. (26) that the ion energy varies in the range of $0 \leqslant \varepsilon_i \leqslant eV_0$. This is the expected result granting the initial assumption for the energy gained by the ion in the sheath. Second, as can be seen from Eq. (29), the IEDF depends on parameter A (31) that determines the ratio between the ion velocities and the moving boundary velocity. In the present approach, A is the only parameter that controls the ion energy spectrum. We have considered the case of $\omega \ll \omega_i$, although the second multiplier in Eq. (31) appears as usual to be much higher than unity: $eV_0 \gg kT_i$. Thus, parameter A may attain values that are higher or less than unity.

Figure 2 presents the IEDF as a function of parameter A in the range from 0 to 60. As can be seen from this figure, the IEDF has a bimodal structure with two pronounced peaks at the points $\varepsilon_i = 0$ and $\varepsilon_i = eV_0$. The low-energy peak decreases and the high-energy peak increases as A increases. The analogous ion spectrum was obtained in [28], in which the IEDF was numerically calculated in the specified electric field. Analyzing expressions (28), (30), and (32), we can also find that the IEDF should have singularities at $\varepsilon_i = 0$ and $\varepsilon_i = eV_0$ because of the zero derivative $d\varepsilon_i/d\varphi$ at these points.

B. Dual frequency discharge: Intermediate frequency regime

In this section, the analytical solution for the IEDF in the DF discharge is considered in the IF case. This task is divided into two steps. First, the rf field will be averaged over HF, and then the procedure described in Sec. A for the LF

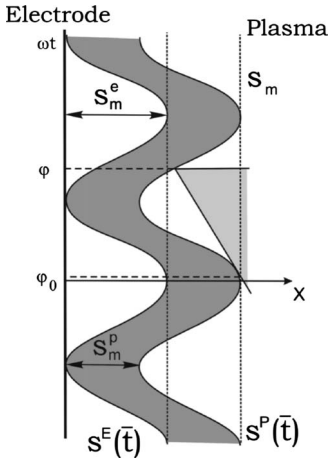

FIG. 3. Diagram of the moving sheath boundary $s_1(t)$ averaged over HF in the DF discharge. $s^e(\bar{t})$ and $s^p(\bar{t})$ are the inner and outer envelope curves; s_m is the maximum sheath width.

case will be repeated using the coarser time scale $\bar{t}$. In this time scale, instead of the sheath boundary $s_1(t)$ that oscillates fast with the frequency ω_h, we introduce two boundaries $s^p(\bar{t})$ and $s^e(\bar{t})$ that are envelopes of $s_1(t)$ (see Fig. 3). $s^p(\bar{t})$ is the boundary between the bulk plasma and the transition zone where the rf field is averaged over HF, $s^e(\bar{t})$ is the boundary between the transition zone and the positively charged space, and the last one is nearer to the electrode. The ion energy gained in the sheath is evaluated by formula (11) as before, but the equation of the boundary motion before averaging over HF in the DF case is determined from Eq. (3). Let us rewrite Eq. (3) in the following form:

$$s_1(t) = \frac{s_m}{2}[\alpha_l(1+\cos\omega_l t) + \alpha_h(1+\cos\omega_h t)], \tag{33}$$

where $\alpha_l = V_l/(V_l+V_h)$, $\alpha_h = V_h/(V_l+V_h)$.

Then the ion energy (11) in the DF case is

$$\varepsilon_i = e\int_{s_1(t)}^{0} E(x,t)dx = eV_0\frac{s_1^2(t)}{s_m^2} = \frac{eV_0}{4}[\alpha_l^2(1+\cos\omega_l t)^2 + 2\alpha_l\alpha_h(1+\cos\omega_l t)(1+\cos\omega_h t) + \alpha_h^2(1+\cos\omega_h t)^2], \tag{34}$$

where $V_0 = V_l + V_h$.

After the averaging of Eq. (34) over HF, the ion energy in the time scale $\bar{t}$ is

$$\varepsilon_i(\bar{t}) = \frac{eV_0}{4}\left(\alpha_l^2(1+\cos\omega_l\bar{t})^2 + 2\alpha_l\alpha_h(1+\cos\omega_l\bar{t}) + \frac{3}{2}\alpha_h^2\right). \tag{35}$$

Then we can write the equations for the outer and inner boundaries $s^e(\bar{t})$ and $s^p(\bar{t})$ as follows:

$$s_e(\varphi) = \frac{s_m^e}{2}[1+\cos(\varphi)], \tag{36}$$

$$s_p(\varphi) = s_m^p + \frac{s_m^e}{2}[1+\cos(\varphi)], \tag{37}$$

where $\omega_l\bar{t} = \varphi$,

$$s_m^e = \alpha_l s_m, \quad s_m^p = \alpha_h s_m. \tag{38}$$

In that way, the ion energy is

$$\varepsilon_i = \frac{eV_l}{\alpha_l}\left(\frac{3\alpha_h^2}{8} + \alpha_h\frac{s_e(\varphi)}{s_m} + \frac{s_e^2(\varphi)}{s_m^2}\right). \tag{39}$$

The subsequent computations are analogous to the SF case. Similar to the SF case, the IEDF calculations in the DF discharge are based on expressions (4) and (5). In the DF case, only the ions coming in phase φ to the external envelope $s^p(\varphi)$ are taken into account. Then, instead of Eq. (18), we have

$$v \geqslant v_{\min} = \frac{\omega_l[s_m - s_p(\varphi)]}{\varphi + 2\pi} = \frac{\omega_l[s_m^e - s_e(\varphi)]}{\varphi + 2\pi}. \tag{40}$$

The dimensionless parameter ξ in the DF case is

$$\xi = \frac{s_e(\varphi)}{s_m^e} = \frac{1}{\alpha_l}\frac{s_e(\varphi)}{s_m}. \tag{41}$$

From Eqs. (39) and (41), we can obtain

$$\xi = -\frac{\alpha_h}{2\alpha_l} + \frac{1}{\alpha_l}\sqrt{\frac{\varepsilon_i}{eV_0} - \frac{\alpha_h^2}{8}}. \tag{42}$$

Parameter ξ should satisfy the following conditions:

$$0 \leqslant \xi, \quad \xi \leqslant 1. \tag{43}$$

From the first inequality, we can obtain

$$\varepsilon_i^{\min} = \frac{3}{8}\alpha_h^2 eV_0, \tag{44}$$

and the second condition gives

$$\varepsilon_i^{\max} = \left(\frac{3}{8}\alpha_h^2 + \alpha_h\alpha_l + \alpha_l^2\right)eV_0. \tag{45}$$

Thus, the range of ion energies is substantially different in comparison with the SF case.

The energy derivative of ξ has the form

$$\frac{d\xi}{d\varepsilon_i} = \frac{1}{\alpha_l eV_0}\frac{1}{2\xi\alpha_l + \alpha_h}. \tag{46}$$

As in the SF discharge, the IEDF is determined by formulas (28)–(32), but in the DF case

$$v_{\min} = \omega_l s_m \alpha_l f_k(\xi), \quad k = 1,2,3, \tag{47}$$

$$C_1(\xi) = \frac{C}{eV_0}\frac{\Gamma_i}{\omega_l\alpha_l}\frac{1}{(2\alpha_l\xi + \alpha_h)\sqrt{\xi(1-\xi)}},$$

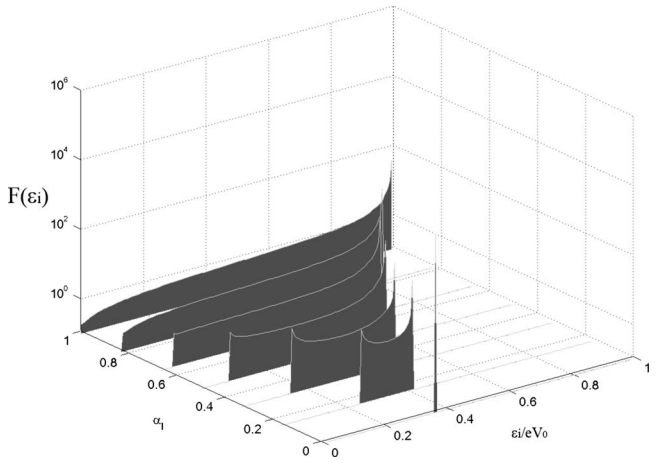

FIG. 4. Analytical IEDF in DF discharge as a function of normalized ion energy $\mathcal{E}_i/eV_0$ and parameter $\alpha_l=V_l/(V_l+V_h)$; the intermediate frequency regime $\tau_h \ll \tau_{ion} \ll \tau_l$ is considered.

$$A = \frac{m\omega_l^2 s_m^2 \alpha_l^2}{2kT_i} = \alpha_l^2 \frac{\omega_l^2}{\omega_i^2} \frac{eV_0}{kT_i}. \tag{48}$$

Besides the ion energy range, the DF case has another difference in comparison with the SF case: the second parameter α_l characterizes the relative contribution of the low and high frequencies.

Figure 4 shows the IEDF as a function of parameter α_l. As can be seen from this figure, the spectrum width decreases as α_l decreases, and in the extreme points it comes to the SF limit. It forms the LF case if $\alpha_l=1$, or the HF case if $\alpha_l=0$.

Figure 5 presents the dependence of $\varepsilon_i^{\min}$ (solid line) and $\varepsilon_i^{\max}$ (dashed line) on parameter α_l.

IV. NUMERICAL SIMULATION

In order to validate the results of the analytical theory, the IEDF was also calculated by using two numerical models.

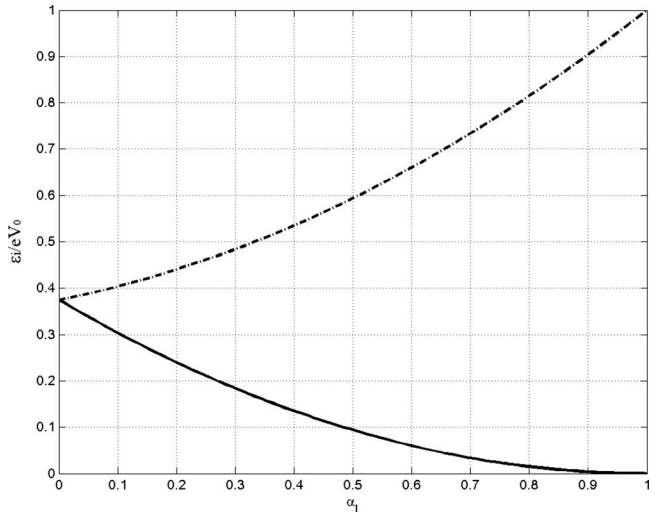

FIG. 5. Positions of the low-energy (solid line) and high-energy (dashed line) peaks of the IEDF in the DF case, calculated with the analytical model as functions of α_l; the intermediate frequency regime $\tau_h \ll \tau_{ion} \ll \tau_l$ is considered.

The first model is a semianalytical extension of the present analytical model. It takes into account the ion collisions with neutrals in the sheath. The second one is a self-consistent numerical model of rf discharge based on the PIC MC approach that allows the simulation of the IEDF formation in the sheath in a situation closest to the real experiments.

A. Semianalytical model

Similar to the above-presented analytical model, the semianalytical model includes expression (1), describing the electric field distribution in the sheath, and Eqs. (2) and (3) of the moving bulk-sheath boundary. The ion collisions with neutral atoms are treated with the MC algorithm.

Ions are generated at the plasma-sheath boundary s_m, and the Maxwellian distribution of ion velocities is assumed with the ion temperature typical for the plasma bulk. Then, ions move through the sheath in the variable electric field $E(x,t)$. When an ion impinges on the electrode, its energy is taken into account in the IEDF calculation.

The present semianalytical model may be expanded for an arbitrary electric field distribution and nonsinusoidal motion of the sheath boundary. In this work, we assume the homogeneous ion density in the sheath, and formulas (1)–(3) are valid in this case.

The probabilities of ion-neutral collisions are calculated using the elastic cross section and charge transfer cross section for Ar^+ [46]. Usage of this set in swarm studies is described in [48].

B. Self-consistent PIC MCC model

In this work, we use the PIC MCC model of the rf discharge that was described in detail in [20]. The charge transfer cross section and elastic cross section for Ar^+ were taken from [46]. The total input power is used as the input parameter in the SF case, and in the DF discharge, the total input power and the LF voltage V_l are supposed to be known. The applied voltage was chosen as a sinusoidal function $V=V_0 \sin \omega t$ in the SF case and as a sum of two sinusoids $V=V_l \sin \omega_l t + V_h \sin \omega_h t$ in the DF case. The V_h value (or V_0 in SF) is adjusted during the calculations until the total input power equals the specified value. It should be noted that V_0, V_l, and V_h are the voltages at the electrode (i.e., an external circuit is not considered here).

V. COMPARISON OF THE ANALYTICAL THEORY AND THE RESULTS OF THE NUMERICAL SIMULATION

In this section, the analytical IEDF will be compared with the results of the PIC MCC model and the semianalytical model. Since the obtained IEDF structure is qualitatively the same for all presented models, we will further focus on the quantitative analysis of the IEDF characteristics as the spectrum width (FWHM), positions of the IEDF peaks, and their height. We will also try to reveal the basic factors that determine the IEDF structure.

The main discharge parameters are presented in Table I. Figure 6(a) shows the IEDF obtained in the PIC MCC simulation of the DF 1.76/81 MHz discharge at an HF voltage of

TABLE I. DF 1.76 MHz–81 MHz discharge parameters. U_p^{PIC}—plasma potential from the PIC modeling, $U_p^{calc}=(3/8)V_0-(V_0/4)\alpha_l\alpha_h+(kT_e/e)$—analytic plasma potential [19].

Discharge parameters					PIC MC results	Analytical model results
V_l (V)	V_h (V)	V_0 (V)	α_l	α_h	U_P^{PIC} (V)	U_P^{calc} (V)
100	150	250	0.40	0.60	100	81.5
100	250	350	0.29	0.71	140	116.2
100	350	450	0.22	0.78	180	152.2
50	250	300	0.17	0.83	128	105.1
150	250	400	0.37	0.63	150	129.5

$V_h=250$ V and three different values of the LF voltage $V_l=50$, 100, and 150 V. The Ar pressure is equal to 20 mTorr in all calculations. Figure 6(b) presents the results of the semianalytical model for the same discharge conditions.

The location of the IEDF peak in the SF case is determined by U_p, as shown in Sec. II. Figure 6(b) illustrates that, in the DF discharge, the low-energy peak is also located near the energy corresponding to the plasma potential of the SF discharge (7) but it is slightly shifted to the lower energies. It

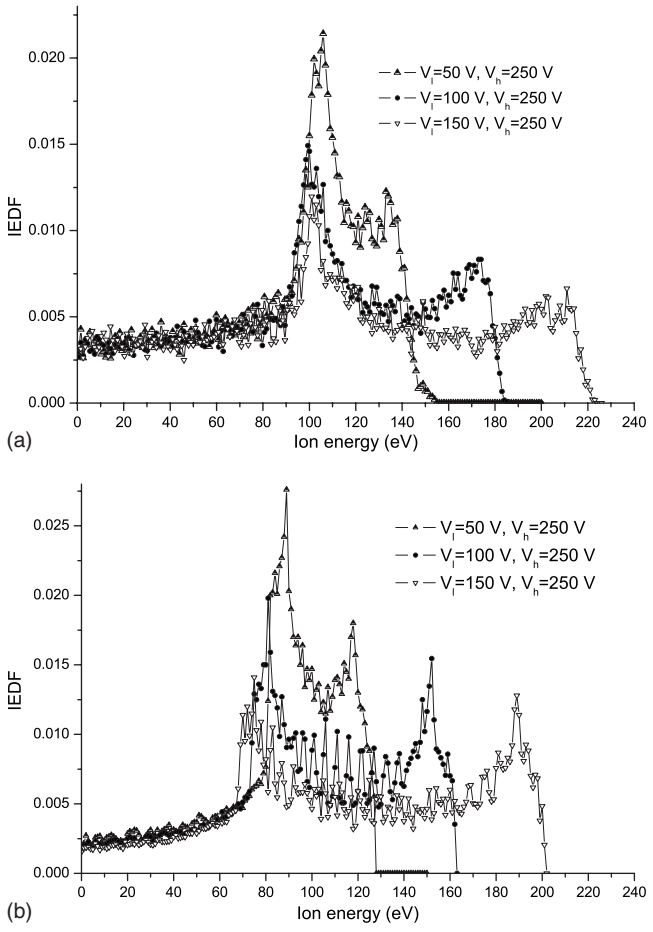

FIG. 6. (a) IEDF in the DF discharge calculated with the PIC MCC model at the constant HF voltage of $V_h=250$ V and different LF voltages $V_l=50$, 100, and 150 V. (b) IEDF in the DF discharge calculated with the semianalytical model at the constant HF voltage of $V_h=250$ V and different LF voltages $V_l=50$, 100, and 150 V.

can easily be understood since expression (44) can be transformed to the following form:

$$\varepsilon_i^{\min}=\alpha_h e U_p^{\text{single}}, \tag{49}$$

where U_p^{single} is the plasma potential in the SF discharge (7), and its value is determined by V_h. It should be noted that both the plasma potential (7) calculated according to the linear theory and the plasma potential in the DF discharge [19] (see Table I) are somewhat lower than the plasma potential obtained in the self-consistent PIC MCC model. Indeed, formula (7) takes into account only the positive charge oscillations in the sheath, and the possible influence of the plasma bulk is beyond the limits of this model. In reality, the ions may enter the sheath with much higher than thermal velocities because of the acceleration in an ambipolar potential. The resulting correction to the plasma potential is evaluated by the following formula [49]:

$$V_{fl}\cong\frac{1}{2}\frac{kT_e}{e}\ln\left(\frac{\pi M_i}{2m_e}\right). \tag{50}$$

In the case of Ar plasma, formula (50) gives

$$V_{fl}\cong 5.8kT_e/e. \tag{51}$$

Here T_e is the electron temperature near the sheath region. In the PIC MCC simulation, kT_e is about 2–4 eV, and V_{fl} may achieve values up to 20 V. Although it is small in comparison with V_l and V_h, the influence of V_{fl} may be noticeable in the exact calculation of the IEDF peak positions.

As can be seen from formula (49), the shift of the low-energy peak is determined by α_h, i.e., the HF component of the applied voltage. In the conditions illustrated in Fig. 6, the HF component is high enough: $0.63<\alpha_h<0.83$. As a result, the positions of the low-energy peaks of the IEDF in Figs. 6(a) and 6(b) are close enough. It should be noted once more that, in contrast with the SF case, the positions of the low-energy and high-energy peaks in the DF discharge do not correlate with the plasma potential U_p^{dual}.

Figures 7(a) and 7(b) present the series of the IEDF calculated at a constant LF voltage $V_l=100$ V and three different values of $V_h=150$, 250, and 350 V. It can be seen from these figures that the position of the low-energy peak changes essentially as V_h is changed, whereas the spectrum width remains almost constant. In that way, according to Eq. (49), the position of the low-energy peak is controlled only by the HF voltage.

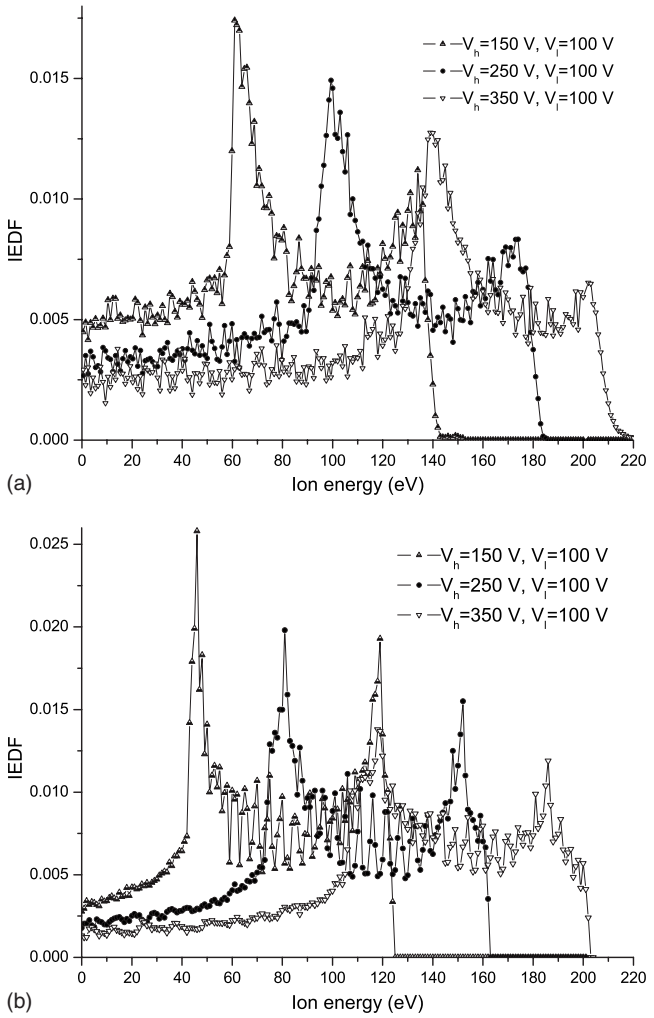

FIG. 7. (a) IEDF in the DF discharge calculated with the PIC MCC model at the constant LF voltage of V_l=100 V and different HF voltages V_h=150, 250, and 350 V. (b) IEDF in the DF discharge calculated with the semianalytical model at the constant LF voltage of V_l=100 V and different HF voltages V_h=150, 250, and 350 V.

Let us analyze the spectrum width and position of the high-energy peak in the DF discharge. Figures 6 and 7 illustrate that the bimodal structure of the IEDF and the spectrum width depend on V_l. The analytical expression for the spectrum width can be found as the difference between Eqs. (44) and (45) as follows:

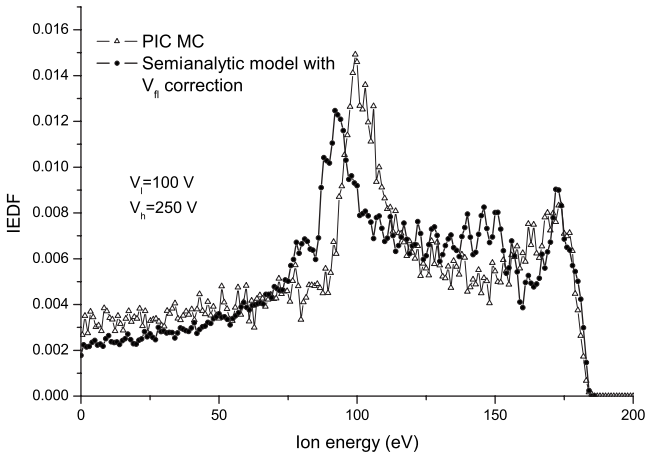

FIG. 8. IEDF in the DF discharge calculated with the PIC MCC model and the semianalytical model (taking into account the correct ion velocity at the sheath boundary; see the text) at HF and LF voltages of V_h=250 and V_l=100 V, respectively.

$$\Delta\varepsilon = \varepsilon_i^{\max} - \varepsilon_i^{\min} = eV_l. \tag{52}$$

The corresponding values of $\Delta\varepsilon$ are presented in Table II. The data presented in Table II also indicate that the ion acceleration in the ambipolar potential has an essential influence on the IEDF structure. The positions of the IEDF peaks obtained in the semianalytical model, taking into account correction voltage V_{fl}, agree well with the PIC MCC results. Nevertheless, it is evident that the higher ion energy at the plasma-sheath boundary should also affect the IEDF at the electrode. In order to test it, we performed the additional simulation by using the semianalytical model, in which the initial ion energy at the plasma-sheath boundary was specified according to Eq. (51). The result of this simulation is presented in Fig. 8 along with the PIC MCC results at the same conditions: V_l=100 V and V_h=250 V. The two ion spectra are almost the same in this case, as can be seen from Fig. 8.

The positions of the IEDF peaks obtained in the analytical theory differ from the simulation results. The analytical low-energy peak is shifted to lower energies and the high-energy peak to higher energies. Thus, the analytical spectrum width is about 15–20% more in comparison with the numerical models. The main reason for this discrepancy is the oversimplification of the ion motion in the sheath in the analytical

TABLE II. IEDF parameters

Discharge parameters		PIC MC			Semianalytical model			Analytical model		
V_l, (V)	V_h	$\varepsilon_i^{\min}$	$\varepsilon_i^{\max}$	$\Delta\varepsilon$	$\varepsilon_i^{\min}$	$\varepsilon_i^{\max}$	$\Delta\varepsilon$	$\varepsilon_i^{\min}$	$\varepsilon_i^{\max}$	$\Delta\varepsilon$
100	150	61.8	134	78	46	119	79	33.8	136.5	100
100	250	99.4	173	82	81	152	80	69.4	170.5	100
100	350	140	209	83	119	186	86	105.2	204.5	100
50	250	104	134	43	89	118	39	80.8	131.5	50
150	250	101	211	118	75	189	130	62.0	210.4	150

model. We assumed that the ions reach the electrode immediately after they enter the sheath region with high electric fields. This is simplification due to the LF limit. In reality, the electric field in the sheath is relatively low for the ions that run into the moving boundary in phase $\varphi \cong 0$. As a result, they do not have time to accelerate and are "overtaken" by the plasma phase again. Thus, these ions will reach the electrode only after one rf cycle and contribute to the low-energy peak of the IEDF (instead of the high-energy peak as in the present analytical model); therefore, they shift the low-energy peak toward higher energies.

It is interesting to make a qualitative comparison of the present analytical model and the other analytical models that are frequently used for the analysis of experimental data. One of these is the model described in [7–9] for the high-frequency limit. The ion spectrum in [7] has the form

$$F(\varepsilon_i) = \frac{2\Gamma_i}{\omega_l \Delta\varepsilon}\left[1 - \left(\frac{2}{\Delta\varepsilon}\right)^2 (\varepsilon_i - e\bar{V}_s)^2\right]^{-1/2}, \qquad (53)$$

and the spectrum width is evaluated by the formula

$$\Delta\varepsilon = e\bar{V}_s \frac{8\lambda_2}{3\bar{s}\omega_l}\left(\frac{2e\bar{V}_s}{M}\right)^{1/2}. \qquad (54)$$

Here $\bar{V}_s$ is the average sheath potential, $\bar{s}$ is the average sheath width, $\lambda_2 \leqslant 1$ is the model parameter, and M is the ion mass. The dependence of the spectrum width on the ion mass in Eq. (54) in the high-frequency limit is one of the main differences between the two models. As follows from Eq. (52) in the intermediate-frequency case $\omega_l \ll \omega_i \ll \omega_h$, the spectrum width is determined by the LF voltage.

The second conclusion of the model [7–9] is that the IEDF at the electrode is symmetrically centered near $e\bar{V}_s$. The above-described analysis shows that it is not correct for intermediate frequencies. This is also confirmed by the results of the numerical simulations presented in this paper, in [12,20], and also by the experimental data [20]. In that way, for the analysis of the IEDF structure, it is important to ascertain which frequency regime is realized in the specific case. It may depend on the rf frequencies ratio, ions mass, HF and LF voltages, and other discharge parameters.

Finally, let us state briefly the influence of ion-neutral collisions on the IEDF. In general, the ion collisions result in the homogeneous low-energy tail in the ion spectrum. This can be seen from the comparison of Fig. 4, in which the results of the collisionless analytical model are shown, and Figs. 6 and 7, which present the results of the PIC MCC and semianalytical models, taking into account ion collisions.

VI. CONCLUSIONS

In this paper, the analytical model of the IEDF formation in the sheath of the DF discharge is presented for the intermediate-frequency limit $\omega_l \ll \omega_i \ll \omega_h$. This regime is most interesting for technological applications. The resulting analytical IEDF was compared with the IEDF calculated by using the PIC MCC model of the DF discharge as well as with the results of the semianalytical model. We can conclude that the analytical approach can be successfully applied for such complicated tasks along with computationally expensive numerical models. The presented analytical model for the DF plasma in the IF case was developed for the first time. In spite of the used simplifications (linear sheath model, constant ion flow), this model allows us to obtain the qualitatively correct IEDF. Analytical expressions for the IEDF peaks position and IEDF width for the IF case allow us to reveal parameters which affect the width of the ion spectrum. Note that the influences of low-frequency voltage on the IEDF width were observed earlier [11], but the analytical formula was not received previously. The quantitative comparison with the numerical models reveals some drawbacks of the analytical model that nevertheless may help to improve it in future work. One of the prospective improvements is a more correct description of the ion motion in the sheath. Another one is taking into account the initial ion velocity at the plasma-sheath boundary caused by the ion acceleration in the ambipolar field.

Finally, let us discuss the idea of frequency decoupling relating to the ion spectrum. The analysis of the obtained ion spectra has shown that pure frequency decoupling is difficult to reach. The spectrum width indeed depends mainly on the LF voltage (without considering ion collisions), but the absolute ion energies and the positions of the IEDF peaks on the energy scale depend on the HF voltage and parameter α_h characterized the ratio of the HF and LF voltages. In that way, even when the electron heating and resulting plasma density are controlled by the HF power, it seems impossible to exclude the influence of the HF power in the ion spectrum. Nevertheless, it is possible to control this influence, and the aim of this work was to find possible ways to do so.

ACKNOWLEDGMENTS

This research was supported by the Russian Foundation of Basic Research (Grant No. 08-02-00465-a) and Key Science School (Grant No. SS-133.2008.2).

[1] J. W. Coburn, *Handbook of Advanced Plasma Processing Techniques* (Springer, Berlin, 2000).
[2] H. H. Goto, H.-D. Lowe, and T. Ohmi, J. Vac. Sci. Technol. A **10**, 3048 (1992).
[3] H. H. Goto, H.-D. Lowe, and T. Ohmi, IEEE Trans. Semicond. Manuf. **6**, 58 (1993).
[4] T. Kitajima, Y. Takeo, and T. Makabe, J. Vac. Sci. Technol. A **17**, 2510 (1999).
[5] T. Kitajima, Y. Takeo, Z. Lj. Petrovic, and T. Makabe, Appl. Phys. Lett. **77**, 489 (2000).

[6] M. A. Lieberman, J. P. Booth, P. Chabert, J. M. Rax, and M. M. Turner, Plasma Sources Sci. Technol. **11**, 283 (2002).
[7] V. Georgieva, A. Bogaerts, and R. Gijbels, Phys. Rev. E **69**, 026406 (2004).
[8] V. Georgieva and A. Bogaerts, Plasma Sources Sci. Technol. **15**, 368 (2006).
[9] V. Georgieva, A. Bogaerts, and R. Gijbels, J. Appl. Phys. **94**, 3748 (2003).
[10] V. Georgieva and A. Bogaerts, J. Appl. Phys. **98**, 023308 (2005).
[11] J. K. Lee, O. V. Manuilenko, N. Yu. Babaeva, H. C. Kim, and J. W. Shon, Plasma Sources Sci. Technol. **14**, 89 (2005).
[12] P. C. Boyle, A. R. Ellingboe, and M. M. Turner, Plasma Sources Sci. Technol. **13**, 493 (2004).
[13] P. C. Boyle, J. Robiche, and M. M. Turner, J. Phys. D: Appl. Phys. **37**, 1451 (2004).
[14] G. Wakayama and K. Nanbu, IEEE Trans. Plasma Sci. **31**, 638 (2003).
[15] F. R. Myers and T. S. Cale, J. Electrochem. Soc. **139**, 3587 (1992).
[16] Z. Guan, Z. Dai, and Y. Wang, Phys. Plasmas **12**, 123502 (2005).
[17] J. Robiche, P. C. Boyle, M. M. Turner, and A. R. Ellingboe, J. Phys. D: Appl. Phys. **36**, 1810 (2003).
[18] R. N. Franklin, J. Phys. D: Appl. Phys. **36**, 2660 (2003).
[19] H. C. Kim, J. K. Lee, and J. W. Shon, Phys. Plasmas **10**, 4545 (2003).
[20] T. V. Rakhimova, O. V. Braginsky, V. V. Ivanov, A. S. Kovalev, D. V. Lopaev, Yu. A. Mankelevich, M. A. Olevanov, O. V. Proshina, A. T. Rakhimov, A. N. Vasilieva, and D. G. Voloshin, IEEE Trans. Plasma Sci. **35**, 1229 (2007).
[21] A. Perret, P. Chabert, J. Jolly, and J.-P. Booth, Appl. Phys. Lett. **86**, 021501 (2005).
[22] C. K. Birdsall, E. Kawamura, and V. Vahedi, *Particle Simulation Methods for Glow Discharges: Past, Present and Future, with Applications*, in Electron Kinetics and Application of Glow Discharges (Plenum Press, New York, 1998).
[23] C. K. Birdsall and A. B. Langdon, *Plasma Physics via Computer Simulation* (McGraw-Hill, New York, 1985).
[24] T. V. Rakhimova, O. V. Braginsky, V. V. Ivanov, T. K. Kim, J. T. Kong, A. S. Kovalev, D. V. Lopaev, Y. A. Mankelevich, O. V. Proshina, and A. N. Vasilieva, IEEE Trans. Plasma Sci. **34**, 867 (2006).
[25] O. V. Proshina, T. V. Rakhimova, and A. T. Rakhimov, Plasma Sources Sci. Technol. **15**, 402 (2006).
[26] Z. Donkó and Z. Lj. Petrovic, Jpn. J. Appl. Phys., Part 1 **45**, 8151 (2006).
[27] Z. Donkó and Z. Lj. Petrovic, J. Phys.: Conf. Ser. **86**, 012011 (2007).
[28] M. J. Kushner, J. Appl. Phys. **58**, 4024 (1985).
[29] M. S. Barnes, J. C. Forster, and J. H. Keller, IEEE Trans. Plasma Sci. **19**, 240 (1991).
[30] B. E. Thompson, H. H. Sawin, and D. A. Fisher, J. Appl. Phys. **63**, 2241 (1988).
[31] T. Panagopoulos and D. J. Economou, J. Appl. Phys. **85**, 3435 (1999).
[32] E. A. Edelberg and E. S. Aydil, J. Appl. Phys. **86**, 4799 (1999).
[33] Z. Dai, Y. Wang, and T. Ma, Phys. Rev. E **65**, 036403 (2002).
[34] Z. Dai, X. Xu, and Y. Wang, Phys. Plasmas **14**, 013507 (2007).
[35] S. Wang, X. Xu, and Y. Wang, Phys. Plasmas **14**, 113501 (2007).
[36] M. A. Lieberman and A. J. Lichtenberg, *Principles of Plasma Discharges and Material Processing* (Wiley, New York, 1994).
[37] M. A. Lieberman, IEEE Trans. Plasma Sci. **16**, 638 (1988).
[38] M. A. Lieberman, IEEE Trans. Plasma Sci. **17**, 338 (1989).
[39] W. Jiang, M. Mao, and Y. Wang, Phys. Plasmas **13**, 113502 (2006).
[40] P. Benoit-Cattin and L. C. Bernard, J. Appl. Phys. **39**, 5723 (1968).
[41] Y. Okamoto and H. Tamagawa, J. Phys. Soc. Jpn. **29**, 187 (1970).
[42] A. Metze, D. W. Ernie, and H. J. Oskam, J. Appl. Phys. **60**, 3081 (1986).
[43] W. J. Goedheer, Plasma Sources Sci. Technol. **9**, 507 (2000).
[44] A. C. F. Wu, M. A. Lieberman, and J. P. Verboncoeur, J. Appl. Phys. **101**, 056105 (2007).
[45] E. Kawamura, V. Vahedi, M. A. Lieberman, and C. K. Birdsall, Plasma Sources Sci. Technol. **8**, R45 (1999).
[46] A. V. Phelps, J. Appl. Phys. **76**, 747 (1994).
[47] Y. P. Raizer, *Gas Discharge Physics* (Springer-Verlag, Berlin, Germany, 1991).
[48] Z. Lj. Petrovic and V. D. Stojanovic, J. Vac. Sci. Technol. A **16**, 329 (1998).
[49] R. W. Boswell and I. J. Morey, Appl. Phys. Lett. **52**, 21 (1988).